DOI: 10.1002/asia.200600134

Photo- and Redox-Active Dendritic Molecules with Soft, Layered Nanostructures

Yoshihiro Kikuzawa,[a] Toshi Nagata,*[a] Tahei Tahara,[b] and Kunihiko Ishii[b]

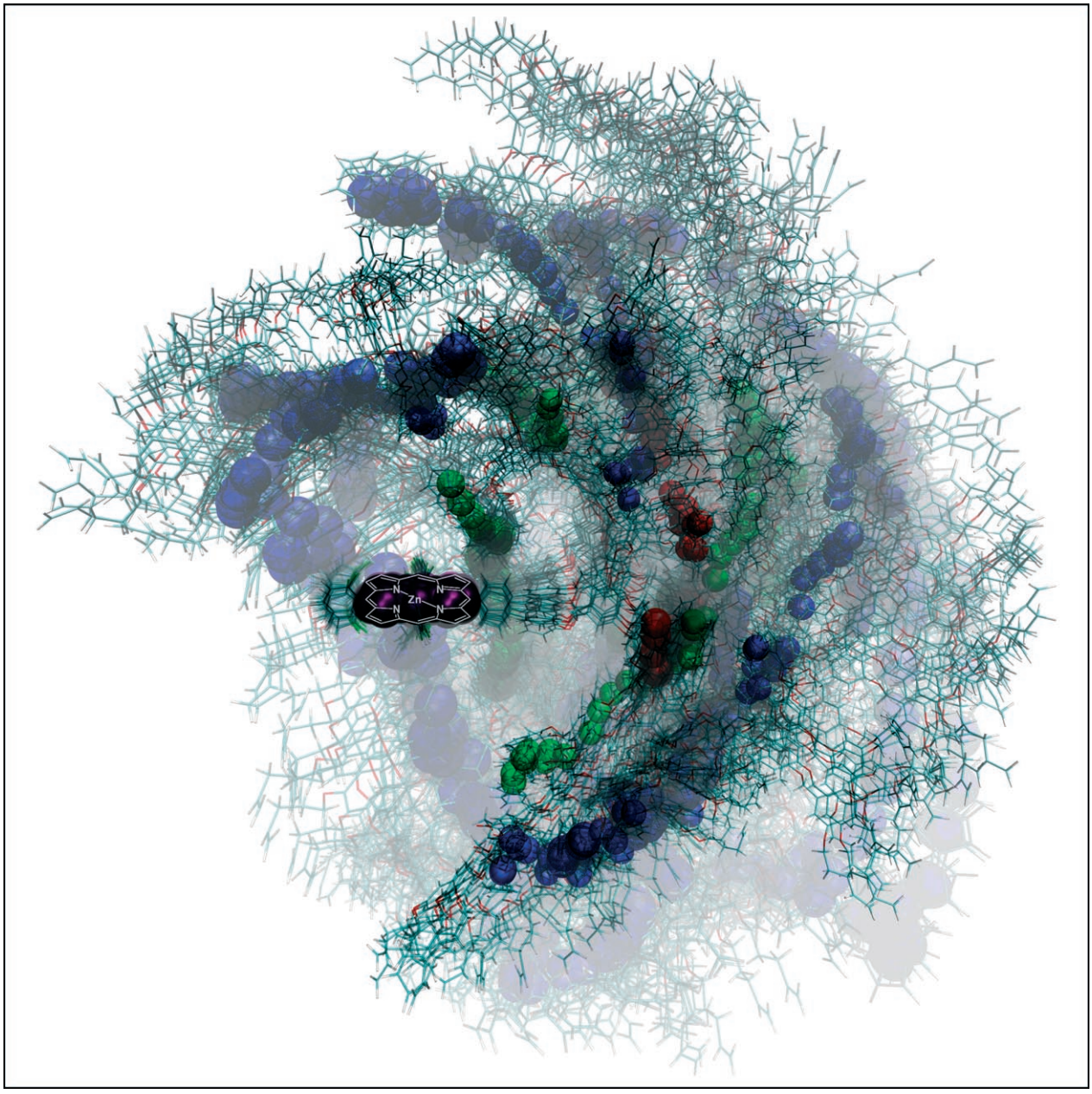

Abstract: Molecules with one photoactive group (porphyrin) and multiple redox-active groups (ferrocenes) are described. The molecules are based on dendritic frameworks, with the ferrocenyl groups attached at the "internal" positions and the porphyrin attached at the focal point, leading to a characteristic layer architecture. Molecules of up to the third generation were synthesized and examined. The results of ^{1}H NMR spectroscopy and fluorescence quenching indicated that the ferrocenyl groups at the second layer approach the core porphyrin most closely, which is consistent with the results of molecular-dynamics simulations. The electrochemistry of the molecules was also examined in detail, and a new formula is proposed for the analysis of multiple-electron transfer in these "redox-pool" molecules.

Keywords: dendrimers · molecular dynamics · nanostructures · porphyrin · redox chemistry

Introduction

Dendrimers with redox-active moieties[1] such as ferrocenes[2] have gained much interest as single-molecule electron pools (molecular batteries),[3] hosts for anion recognition,[4] and electrochemical biosensors.[5] One particularly interesting application is the introduction of a photoactive group into such multiple redox-active molecules. Indeed, there are reports of dendrimers that have a photoactive (e.g., porphyrin) group at the core and multiple redox-active groups attached to the dendritic framework.

These types of molecules can be classified into two categories based on the positions at which the redox-active moieties are attached. In the first, the redox-active groups are attached at the periphery of the dendrimer (Figure 1, left).[6] Although this design is simple, its weakness is that the peripheral groups become farther from the core group as the generation becomes higher. When photoinduced electron transfer takes place in the high-generation compounds, the electron must travel large distances across the dendrimer framework.

In the second category, the redox-active moieties are attached at the internal positions of the dendrimer (Figure 1, right). Redox-active dendrimers of this type of "layered" structure (not necessarily containing photoactive groups at the core) have been reported with ferrocenes,[7] tetrathiafulvalenes,[8] pyridiniums,[9] carbazoles,[10] arylamines,[11] and Ru^{II} complexes[12] as the redox-active moieties. The phenylazomethine dendrimers of Yamamoto and co-workers are of a particularly elegant design: they sequentially bind metal ions layer by layer.[13] In these layered structures, some of the redox-active moieties are always close to the photoactive moiety at the core, and the redox-active moieties are allowed to accumulate as the generation number increases. Similar layered dendrimers are also utilized for vectorial excitation transfer to the core chromophore.[14]

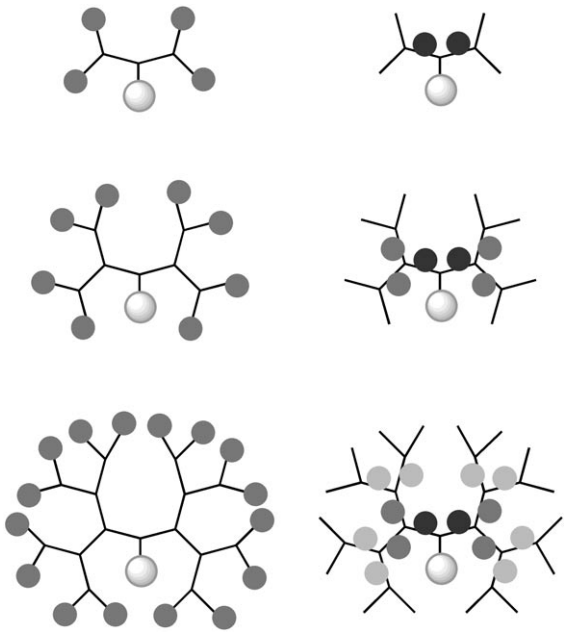

Figure 1. Schematic representation of the dendrimers with one photoactive group at the core and multiple redox-active groups at the periphery (left) and at the inside positions (right).

[a] Y. Kikuzawa, T. Nagata
National Institutes for Natural Science (NINS)
Institute for Molecular Science (IMS) and
Department of Structural Molecular Science
Graduate University for Advanced Studies (Sokendai)
5-1 Higashiyama, Myodaiji, Okazaki 444-8787 (Japan)
Fax: (+81) 564-59-5510
E-mail: toshi-n@ims.ac.jp

[b] T. Tahara, K. Ishii
The Institute of Physical and Chemical Research (RIKEN)
2-1 Hirosawa, Wako, Saitama 351-0198 (Japan)

Supporting information for this article is available on the WWW under http://www.chemasianj.org or from the author.

Most of the "layer"-type dendrimers described above have one common structural architecture: the redox-active groups are introduced as the part of the dendritic framework. This design has its own merit (like rigid, controllable overall structures), but its problem is that we cannot easily change the redox-active groups without changing the overall structure. On the other hand, it is common in the "peripheral"-type redox-active dendrimers that the redox-active groups are introduced at the last stage by use of the reactive functional groups (such as NH_2, CO_2H, etc.) at the end of the dendritic framework. This allows us to change the redox-active groups while keeping the dendritic framework the same.

Previously, we reported the synthesis of dendrons that contain carboxylic esters at the internal positions.[15] Such dendrons are useful for preparing the "layer"-type dendrimers with various redox groups at the internal positions. Herein, we report such dendrimers with internal ferrocenyl groups and a porphyrin at the core (Figure 2). We prepared dendrimers up to the third generation, with fourteen ferrocenyl groups. The three nonequivalent types of ferrocenyl groups were distinguished by ^{1}H NMR spectroscopy. The effects of these ferrocenyl groups on the fluorescence of the core porphyrin were accumulative. We also performed a molecular-dynamics simulation of these molecules with explicit solvent, which revealed the characteristic "soft and layered" distribution of the internal ferrocenyl groups.

Results and Discussion

Synthesis

Schemes 1–3 show the synthetic scheme of the target compounds G*n*(Fc)$_m$-ZnPn (where *n* and *m* denote the generation and the number of ferrocenyl groups, respectively). One of the improvements over our previous synthetic route[15] is the successful preparation of **4**. Compared with the previous procedure, which included alternate reactions of 5-methoxycarbonyl-3-hydroxybenzyl alcohol and 3,5-dihydroxybenzyl alcohol, the number of steps for building a dendritic framework of any given generation are reduced to half. Compound **4** is a stable white solid that can be stored at room temperature for months without decomposition. The starting material **1** is also an easy-to-handle crystalline compound (although it should be stored dry and cold be-

Abstract in Japanese:
1つの光活性基（ポルフィリン）と複数の酸化還元活性基（フェロセン）を含む分子について調べた。これらの分子はポルフィリンをコア部に持つデンドリマーであり、フェロセニル基はデンドリマー骨格の「内部」に結合している。第3世代までの化合物を合成した。^{1}H NMR および蛍光消光の結果から、第二層のフェロセニル基がポルフィリンに最も近付くことが示唆され、これは分子動力学計算の結果とも一致した。電気化学についても詳細に調べ、このような「酸化還元プール」の多段階電子移動を正しく解析する新しい計算式を提案した。

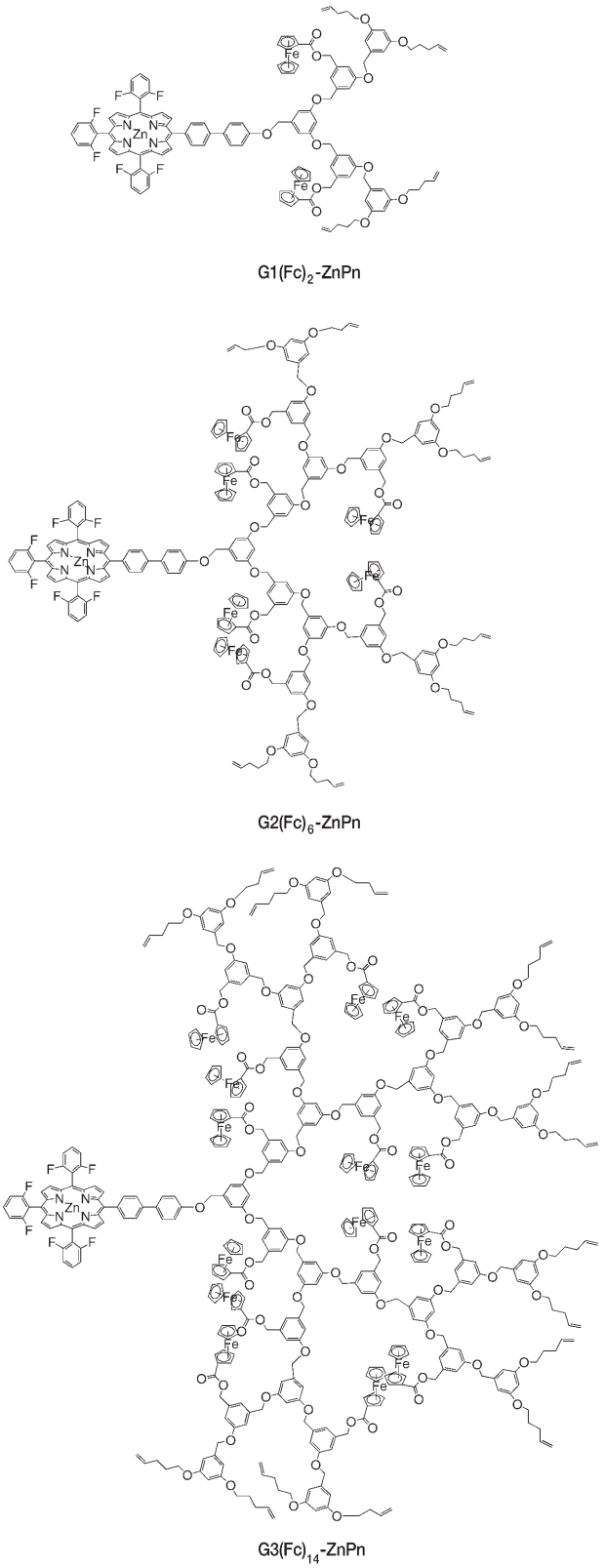

Figure 2. The target molecules in this study. G = generation, Pn = porphyrin, Fc is defined in Scheme 3.

CHEMISTRY
AN ASIAN JOURNAL

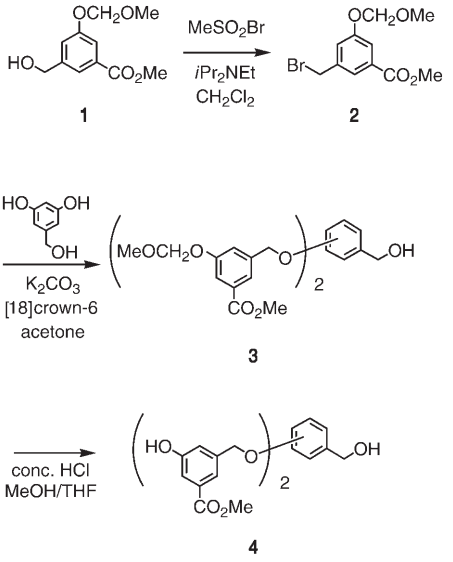

Scheme 1. Synthesis of the dendron precursors.

cause the methoxymethyl ether function causes slow decomposition at room temperature) and can readily be prepared on a multigram scale. Thus, the preparation of a whole series of these dendrimers is easy once these key compounds are at hand.

Another improvement is the use of methanesulfonyl bromide[16] for conversion of benzylic alcohols to bromides. In the synthesis of dendrimers with aryl benzyl ether linkages, the most popular methods are bromination with CBr_4/PPh_3 followed by Williamson ether synthesis,[17] and the direct reaction of benzylic alcohol with phenols by the Mitsunobu reaction.[18] Both methods often suffer from difficulty in removal of stoichiometric amounts of the by-products ($POPh_3$ and $CHBr_3$ in the former and hydrazocarboxylic ester in the latter case). Methanesulfonyl bromide has only rarely been used for the preparation of bromides from alcohols,[19] but its advantage is that the procedures are simple and the reaction is atom-economical.

Characterization

Figure 3 shows parts of the ^{1}H NMR spectra of Gn(Fc)$_m$-ZnPn that include the signals of the ferrocenyl groups. The three signals of these groups, H_a, H_b, and H_c, were observed, and the compounds G2(Fc)$_6$-ZnPn and G3(Fc)$_{14}$-ZnPn gave clearly resolved signals corresponding to each layer of the dendritic framework. Notably, the signals of the ferrocenyl groups at the second layer appear most upfield, followed by those at the third and the first layers. A reversal of this order is probably caused by the structures of these molecules in solution (see below).

Electrochemistry

Figure 4 shows the differential pulse voltammograms of Gn(Fc)$_m$-ZnPn in CH_2Cl_2 with Bu_4NClO_4 (0.1 mol dm^{-3}) as a supporting electrolyte. All compounds showed three oxidation peaks at 0.2, 0.5, and 0.7 V (vs. $[FeCp_2]/[FeCp_2]^+$; Cp = cyclopentadienyl). The peaks at the lowest potential (peak I) grew as the number of ferrocenyl groups was increased, which suggests that this peak corresponds to the oxidation of the ferrocenyl groups. The two peaks at higher potentials (peaks II and III) correspond to the oxidation of

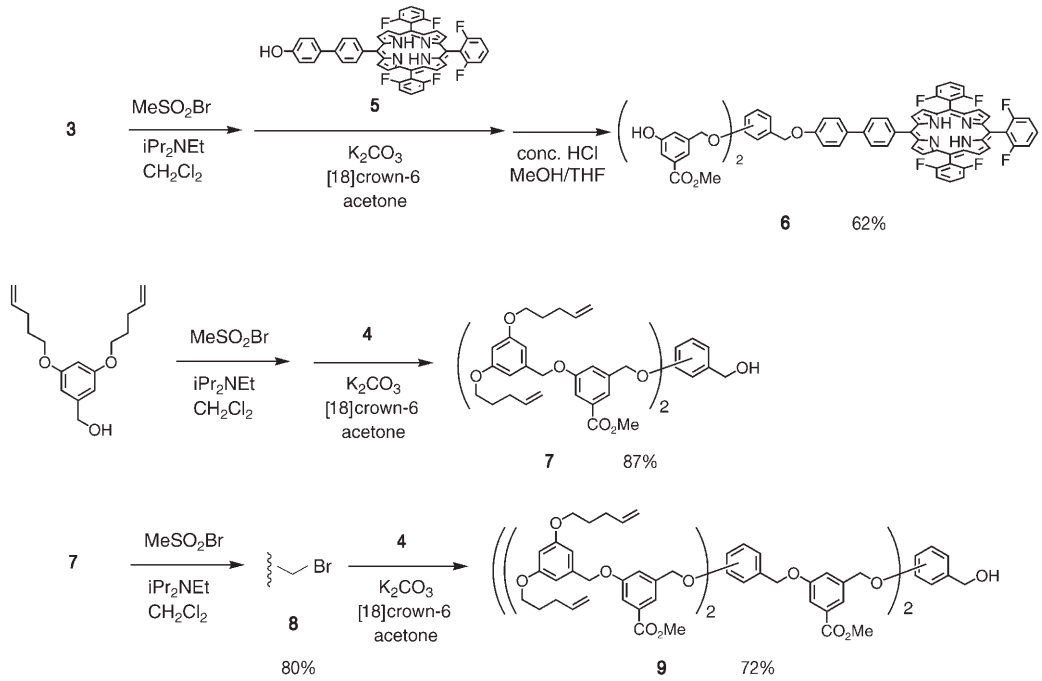

Scheme 2. Synthesis of the dendrons and the porphyrin derivative for the core.

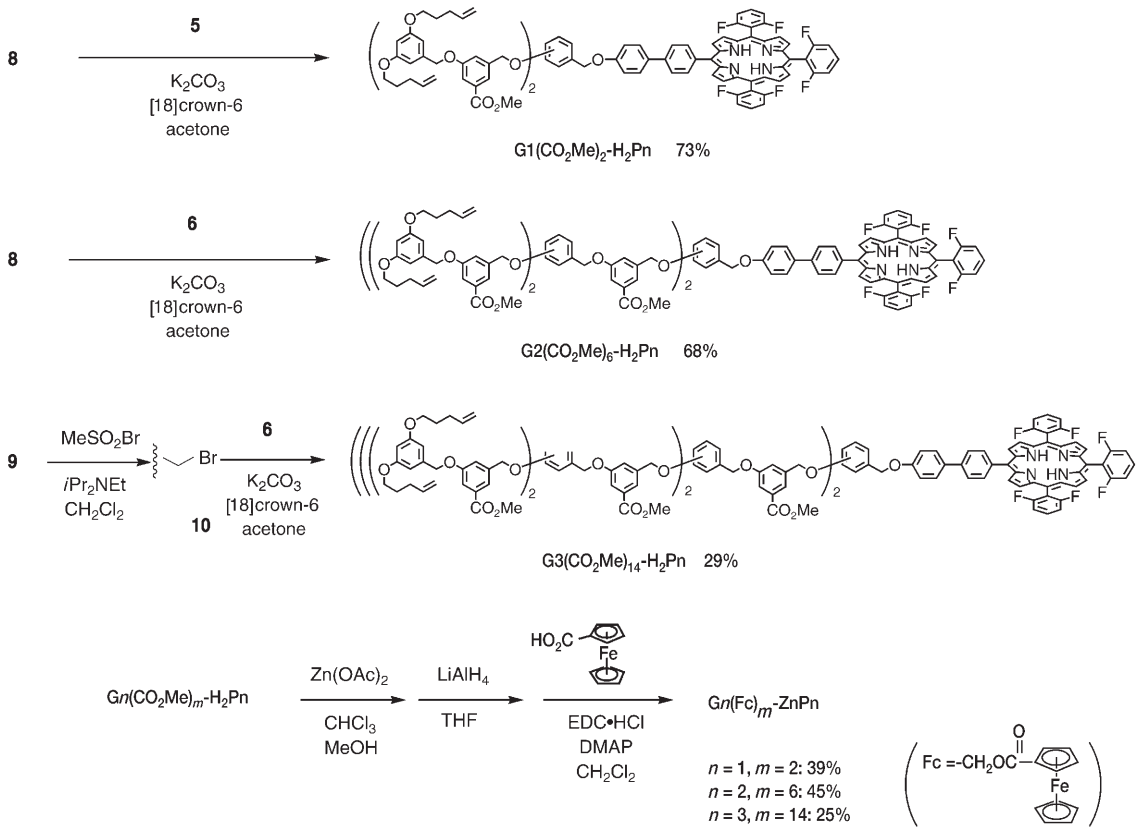

Scheme 3. Synthesis of the target dendrimers. DMAP = 4-dimethylaminopyridine, EDC = *N*-ethyl-*N*′-(3,3-dimethylaminopropyl)carbodiimide.

the porphyrin ring at the core. This is confirmed by comparison of the voltammograms with that of the reference compound Bn-ZnPn (Figure 4).

At first glance, the relative heights of peaks I and II seem to correspond to the number of ferrocenyl groups in the molecule. However, the interpretation was not so straightforward because of the strong dependence of the relative peak heights on the pulse widths (Δt) of the differential pulse voltammetry (DPV) measurements. Figure 5 shows the voltammograms of G1(Fc)$_2$-ZnPn with a series of different pulse widths, and Figure 6a shows a plot of the peak heights versus $(\Delta t)^{-1/2}$. The pulse widths define the electrochemical timescale of the DPV measurements, and the theories of electrochemistry predicts that, in ideally reversible (i.e., electron transfer is much faster than mass transfer) systems, the peak current (I_{max}) in DPV is proportional to $(\Delta t)^{-1/2}$.[20] As shown in Figure 6a, the plot of I_{max} versus $(\Delta t)^{-1/2}$ is linear for peak II, but that for peak I is noticeably bent. Figure 6b and c show similar plots for G2(Fc)$_2$-ZnPn and G3(Fc)$_{14}$-ZnPn, respectively, and the plots for peak II become more bent as the number of ferrocenyl groups is increased.

To account for the bent plots for peak I, we carried out numeric simulations of the voltammograms. The following model is assumed: the $N+1$ oxidation states of the molecule (N = number of ferrocenyl groups) coexist in solution, and the elementary electrode process includes transfer of only one electron to change the oxidation state by one. The mathematical treatment of this system is given in the Supporting Information. We obtained the best-fit plots for peaks I and II by optimizing D (the diffusion constant of the molecule; assumed to be equal for all oxidation states) and k_1 and k_2 (the heterogeneous rate constants for oxidation of a single ferrocenyl group and the porphyrin ring, respectively). The calculated results are shown in Figure 6 (dotted lines), and the optimized parameters are shown in Table 1.

The calculated results reveal two points. First, the rates of electron transfer are slower for the ferrocenyl groups than for the porphyrins. The electrochemical oxidation of ferrocenes is usually fast with $k = 10^{-1}$–10^{-2} cm s^{-1}.[21] The observed rate constants are about one order of magnitude lower. This observation can be attributed to the molecular architecture, in which the ferrocenyl groups are embedded within the dendritic framework. A similar phenomenon was reported by Cardona and Kaifer for a series of dendrimer-substituted ferrocenes,[22] as well as for other dendrimers with redox-active groups at the core.[23] Second, the degree of nonlinearity of the I_{max} versus $(\Delta t)^{-1/2}$ plots is related to N. To emphasize this point, Figure 7 shows three calculated I_{max} versus $(\Delta t)^{-1/2}$ plots that differ only in N. We can clearly see that the shapes of the curves are dependent on N.

Leventis et al. reported that, in their redox-active dendrimers, the number of electrons transferred under voltammetric conditions was less than the number of redox-active

CHEMISTRY
AN ASIAN JOURNAL

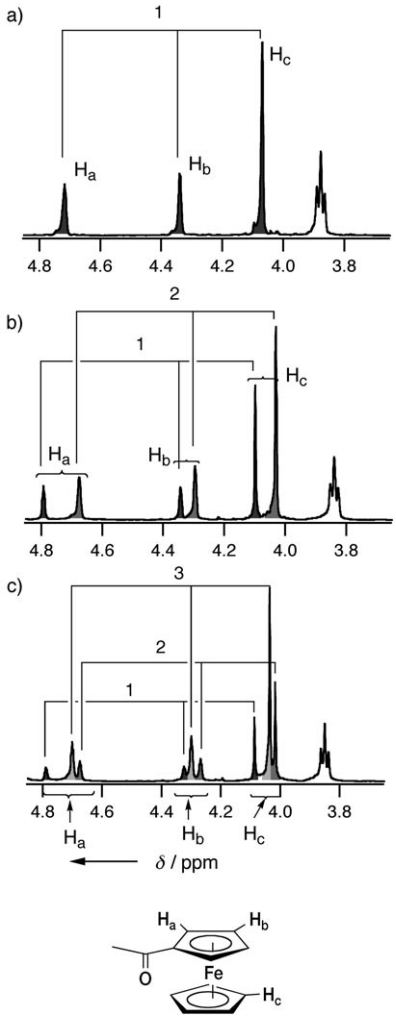

Figure 3. ^{1}H NMR spectra of a) G1(Fc)$_2$-ZnPn, b) G2(Fc)$_6$-ZnPn, and c) G3(Fc)$_{14}$-ZnPn. Only the regions of the ferrocene-ring protons are shown. The signals corresponding to the first, second, and third layers are labeled as 1, 2, and 3, respectively.

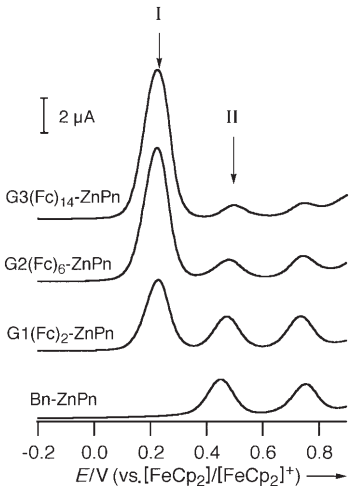

Figure 4. Differential pulse voltammograms of the dendrimers and reference compounds. The peaks labeled I and II are for oxidation of the ferrocenyl groups and the porphyrin, respectively. Pulse width = 42 ms.

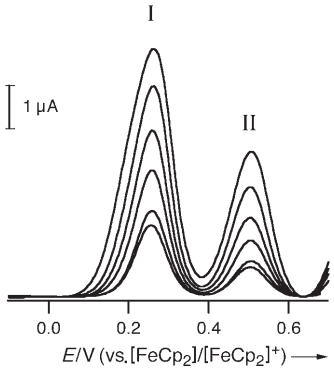

Figure 5. Differential pulse voltammograms of G1(Fc)$_2$-ZnPn with various pulse widths. The pulse widths are 5, 10, 20, 42, 83, 167 ms (bottom to top).

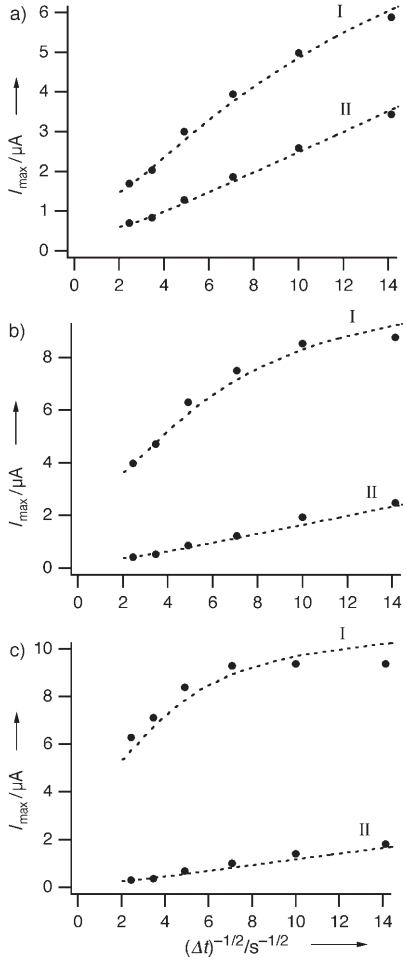

Figure 6. Plots of DPV peak heights versus $(\Delta t)^{-1/2}$. a) G1(Fc)$_2$-ZnPn, b) G2(Fc)$_6$-ZnPn, c) G3(Fc)$_{14}$-ZnPn. The labels I and II correspond to the labels in Figure 4. ● = Experimental, -----= calculated.

Table 1. Electrochemical parameters of the dendrimers obtained from the DPV results.

Compound	D [m^{2}s^{-1}]	k_1 [cms^{-1}]	k_2 [cms^{-1}]
G1(Fc)$_2$-ZnPn	1.7×10^{-10}	9.6×10^{-3}	4.0×10^{-2}
G2(Fc)$_6$-ZnPn	7.5×10^{-11}	7.2×10^{-3}	3.0×10^{-2}
G3(Fc)$_{14}$-ZnPn	4.1×10^{-11}	6.0×10^{-3}	6.3×10^{-2}

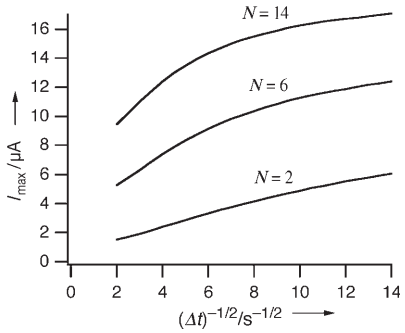

Figure 7. Calculated DPV peak heights with the same parameters (D=1.7×10^{-10} m s^{-2} and k=9.6×10^{-3} cm s^{-2}) but different number of redox-active groups (N).

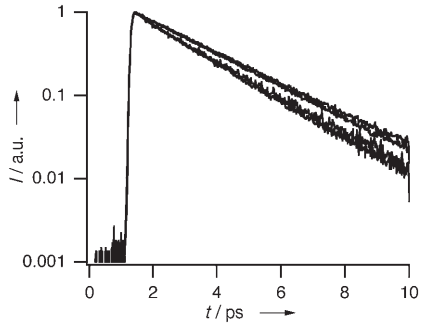

Figure 8. Time-dependent changes in the fluorescence intensities of Bn-ZnPn, G1(Fc)$_2$-ZnPn, G2(Fc)$_6$-ZnPn, and G3(Fc)$_{14}$-ZnPn in toluene. The detection wavelength was 500–750 nm.

groups in the molecule.[9] In our case, we did not see any evidence of such behavior. More rigorously speaking, our electrochemical model can explain the observed results without considering the apparent number of redox-active groups. On the other hand, if the ferrocenyl groups were only partially oxidized in peak I, it would be unlikely that the first oxidation peak of the porphyrin (peak II) would show the clean, reversible one-electron electrochemistry as observed. Therefore, we propose that our analysis represents the electrochemistry of our system sufficiently.

We can summarize the implication of the above analysis as follows. In these types of redox-pool molecules, the DPV measurements at different pulse widths are very informative. By analyzing the voltammograms appropriately, it is possible to assess both the rate of electron transfer and the number of redox-active moieties.

Fluorescence Quenching

In these compounds, the fluorescence of the porphyrin was partially quenched by the ferrocenyl groups. The degree of quenching increased with solvent polarity (data not shown), which is consistent with the quenching mechanism of electron transfer from the ferrocenyl group (donor) to the porphyrin (acceptor). The presence of the electron-withdrawing 2,6-difluorophenyl substituents facilitates this electron transfer, as a similar compound with 3,5-di-*tert*-butylphenyl substituents showed no fluorescence quenching (data not shown).

The fluorescence quenching became stronger as the number of ferrocenyl groups increased, which indicates the accumulative effect of each ferrocenyl layer up to the third generation. Figure 8 shows the temporal profiles of the time-resolved fluorescence. All profiles fitted well to the monoexponential function. Table 2 lists the fluorescence lifetimes (τ) and apparent quenching rate constants ($k_{app}=1/\tau-1/\tau_0$; τ_0=lifetime of reference compound Bn-ZnPn) obtained. With the assumption that each ferrocenyl group contributes to the quenching independently, and that all the ferrocenyl groups in the same layer contribute equally, the contribution of one ferrocenyl group in each layer can be calculated as follows:

Table 2. Fluorescence lifetimes and apparent quenching rate constants of the dendrimers.

Compound	τ [s]	k_{app} [s^{-1}]
Bn-ZnPn	2.33×10^{-9}	–
G1(Fc)$_2$-ZnPn	2.23×10^{-9}	1.92×10^{7}
G2(Fc)$_6$-ZnPn	1.95×10^{-9}	8.36×10^{7}
G3(Fc)$_{14}$-ZnPn	1.84×10^{-9}	11.4×10^{7}

First layer: $k_1=1.92\times10^7/2=0.96\times10^7$ s^{-1};
Second layer: $k_2=(8.36-1.92)\times10^7/4=1.61\times10^7$ s^{-1};
Third layer: $k_3=(11.4-8.36)\times10^7/8=0.38\times10^7$ s^{-1}.

The second layer had the largest effect per ferrocenyl group. This reversal of order is similar to that observed in the ^{1}H NMR chemical shifts and can also be attributed to the structures of these molecules in solution.

Molecular Dynamics

To estimate the average structures of these large, flexible molecules, we carried out molecular-dynamic (MD) simulations of these molecules in $CHCl_3$. A common problem in simulations of molecules of this size is the slow movement of the backbone, the dendritic framework in the present case. This tends to restrict the movements of the ferrocenyl groups on the side chains and to cause ambiguity about their mutual orientations. To avoid this ambiguity, we first ran the simulation without solvents and considered only short-range interactions. Free from solvation and long-range interactions, the molecule easily samples various conformations during a relatively short time. More importantly, this preliminary simulation gave an approximate distribution of the possible structures, as no specific long-range interactions and solvation are expected to affect the structures of the present molecules. Next, a series of productive simulations were performed with initial structures randomly selected

from the trajectory of the preliminary simulations. The results were then combined to give an ensemble of conformations at 300 K. The combined ensemble showed that, for each layer of ferrocenes, the topologically equivalent iron atoms (i.e., the two, six, and 14 Fe atoms in the first, second, and third layers, respectively) gave similar spatial distributions (the plots are found in the Supporting Information). This suggests that the conformations of the dendritic framework were sampled over sufficiently wide variations to allow mutual exchange of equivalent ferrocenyl groups.

Figure 9 shows the spatial distribution of the iron atoms of all the ferrocenyl groups in relation to the porphyrin ring at the core. Each point corresponds to one structure in the ensemble. Figure 10 shows the radial distribution functions of the iron atoms in the first, second, and third layers from the center of the porphyrin ring. These figures clearly show that only the ferrocenyl groups in the second layer have significant probability to approach the porphyrin ring closer than 10 Å. This observation is consistent with the results of ^{1}H NMR spectroscopy and fluorescence quenching, namely,

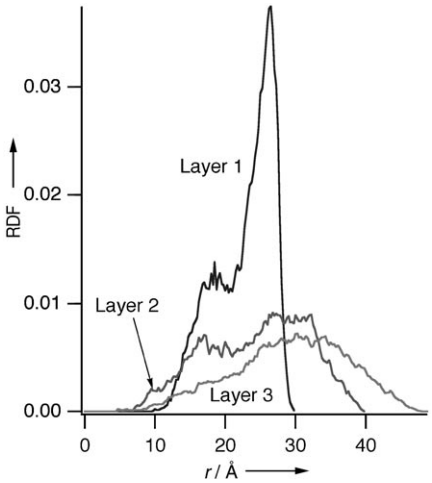

Figure 10. Radial distribution function (RDF; per single atom) of the iron atoms in each layer in G3(Fc)$_{14}$-ZnPn.

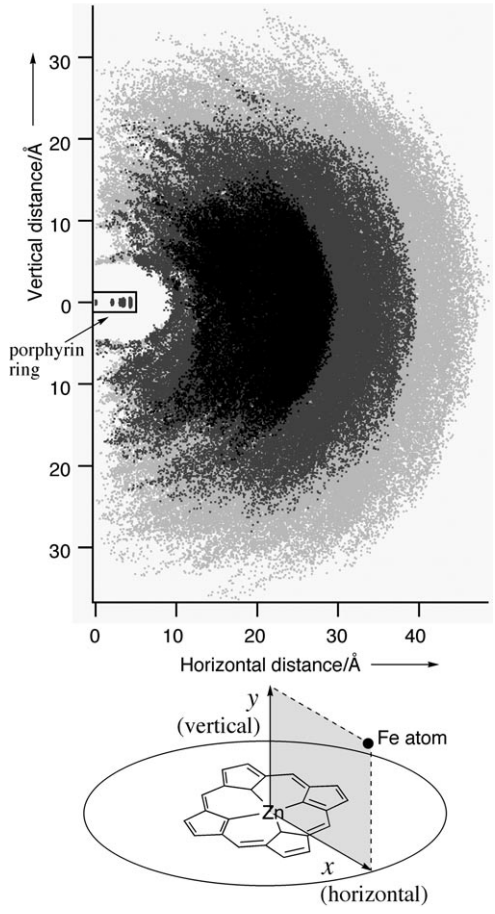

Figure 9. Calculated distribution of the iron atoms of the ferrocenyl groups in G3(Fc)$_{14}$-ZnPn. The three-dimensional atom positions are projected onto the two-axis graph by in-plane (horizontal) and out-of-plane (vertical) distances from the center of the porphyrin ring. The first, second, and third layer are represented by dark gray, medium gray, and light gray, respectively.

the second layer has a larger interaction with the porphyrin ring than the first and third layers. In spite of the soft, flexible nature of the dendritic framework, the side-chain groups still retain the layered distribution in the averaged structure.

Interestingly, such layered distribution was more distinct in G3(Fc)$_{14}$-ZnPn than in G2(Fc)$_6$-ZnPn. The spatial distribution and radial distribution functions of the iron atoms in G2(Fc)$_6$-ZnPn also showed similar trends to G3(Fc)$_{14}$-ZnPn, although the distribution of the first-layer Fe atoms was somewhat broader in G2(Fc)$_6$-ZnPn than in G3(Fc)$_{14}$-ZnPn (see Supporting Information). These results suggest that, even in the case of these "spatially relaxed" dendritic frameworks, the presence of the higher-generation branches restricts the movements of the inner layer.

We also carried out MD simulations of a solution of G3(Fc)$_{14}$-ZnPn with Bu_4NClO_4 in $CHCl_3$ to account for the dynamics of electrochemistry. Our aim was to clarify whether the ferrocenyl groups were really "buried" inside the framework, and by how much. To answer this question, we needed to know where the ferrocenyl groups are located when the molecule approaches the planar electrode. This is described as the distribution function along the normal of the planar electrode, that is, the probability of a certain atom at distance r from the electrode plane. This function is simply estimated from the MD results in solution by assuming an imaginary plane of a random orientation that touches the molecule at a single point and calculating the distance of the atom of interest from this plane. Figure 11 shows the distribution functions of the Fe atoms of the ferrocenyl groups (averaged over 14 Fe atoms) and the Zn atom of the porphyrin. There is a spike at 2.6 Å in the Fe distribution curve. This corresponds to the ferrocenyl group exposed at the "surface" of the molecule. However, the fraction of Fe atoms in this spike is small (the integrated probability for 0–3.0 Å was less than 2%), and the rest of the Fe atoms are distributed at 3–50 Å with a broad maximum at 22 Å. On

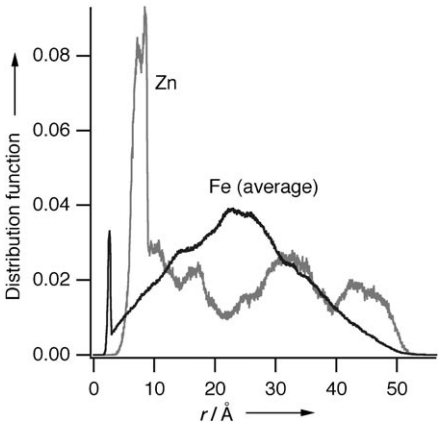

Figure 11. Axial distribution function (per single atom) of the iron atoms (average for all layers) and the zinc atom.

the other hand, the distribution of the Zn atom has a broader peak at 7–9 Å, which accounts for about 20% of the Zn atoms. The broadness and height of the peak are attributed to the larger size and anisotropy of the porphyrin ring relative to the ferrocenyl group. The functions in Figure 12 thus clearly indicate that the porphyrin ring is more likely to approach the electrode than the ferrocenyl groups. This may be one reason for the slow electron transfer of the ferrocenyl groups found in the DPV analysis. Smith and Gorman reported a similar analysis of electrochemical results in combination with the MD simulations.[24] They discussed several lowest-energy conformations and successfully explained the observed differences between rigid and flexible dendrimers. On the other hand, our analysis is based on the axial distribution functions, which gives us the advantage of visualizing

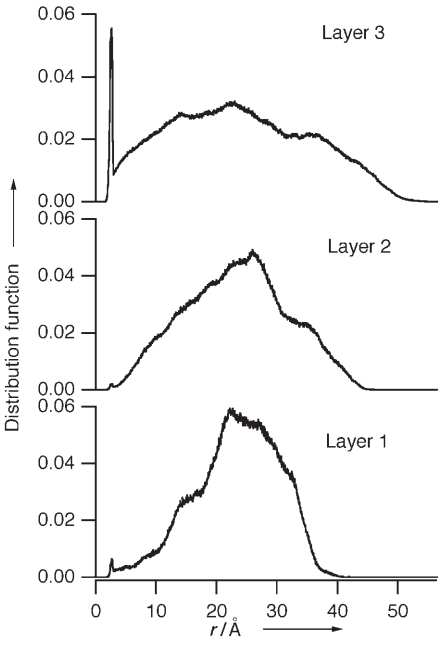

Figure 12. Axial distribution function (per single atom) of the iron atoms in each layer.

the time-averaged distributions of many ferrocenyl groups at once.

So far, we have deliberately ignored the layer dependence of the ferrocenyl groups and discussed only the averaged distribution, because our electrochemical results were not suitable for discrimination of the ferrocenyl groups in different layers. However, we can also calculate the distribution of each layer of ferrocenes from the MD results, which is shown in Figure 12. The spike at 2.6 Å is much more evident for the third layer than for the others, and the ferrocenyl groups of the first and second layers have almost no direct interaction with the electrode. This suggests that the electrochemical oxidation of the ferrocenyl groups of the first and second layers may proceed by electron exchange with the ferrocenyl groups in the third layer, rather than by direct electron transfer with the electrode. Although the present work does not give any clues as to whether this is the case, this is an interesting possibility that deserves further study.

Conclusions

We have prepared dendrimers with a porphyrin ring at the core and ferrocenyl groups at the internal positions in the framework up to the third generation. The synthetic route was improved over that in our previous report to allow faster, more-efficient synthesis. The solution structures were characterized by the NMR spectroscopic signals of the ferrocenyl groups, and the results were consistent with those of the fluorescence-quenching experiments and the MD simulations. We have also proposed a new method for the analysis of electrochemical results. These results and techniques will provide the basis for the development of more-complex and sophisticated soft, layered nanomaterials based on this type of molecule.

Experimental Section

General

Tetrahydrofuran (THF) and diethyl ether were distilled from sodium diphenylketyl. Dichloromethane was distilled from calcium hydride. Other chemicals were used as received. ^{1}H, ^{13}C, and ^{19}F NMR spectra were recorded on JEOL LA500 and LA400 spectrometers. For ^{1}H and ^{13}C NMR spectroscopy, the solvent signals were used as the internal reference. For ^{19}F NMR spectroscopy, C_6F_6 in $CDCl_3$ was used as the external reference ($\delta = 164.9$ ppm vs. $CFCl_3$). Melting points were determined with a Yanaco MP-500V instrument (uncorrected values). UV/Vis spectra were recorded on a Shimadzu UV-2500PC spectrometer. Fluorescence-emission spectra were recorded on a Shimadzu RF-5300PC spectrometer. MALDI-TOF MS spectra were recorded on an Applied Biosystems Voyager System 4174 instrument operating at 20 kV accelerating voltage and positive-ion mode, with dithranol matrix and $CHCl_3$ solvent. Medium-pressure column chromatography was carried out with a Wakogel C-200 instrument. Analytical thin-layer chromatography (TLC) was performed on Merck TLC aluminum sheets (silica gel RP-18 F_{254}). Preparative gel-permeation chromatography (GPC) was performed on an LC-908 (Japan Analytical Industries) system with polystyrene-based columns (JAIGEL-2.5H and -2H) and $CHCl_3$ (3.5 mL min^{-1}) at room temperature. The retention times (t) are reported for each step. The term "the usual workup"

in the synthetic procedures means "water was added to the reaction mixture, and the product was extracted with ethyl acetate, washed with water and brine, dried over anhydrous sodium sulfate, and the solvent evaporated." The data for the compounds (melting points, $^{1}H/^{13}C/^{19}F$ NMR, elemental analysis, HRMS) are listed in the Supporting Information.

Synthesis of Dendrimer Precursors

Dimethyl 5-methoxymethoxybenzene-1,3-dicarboxylate: A suspension of dimethyl 5-hydroxybenzene-1,3-dicarboxylate (21.0 g, 0.10 mol) in THF (120 mL) was placed in a three-necked flask (500 mL) equipped with two dropping funnels. One dropping funnel was filled with a solution of potassium hydroxide (85%, 13.2 g, 0.20 mol) in water (30 mL), and the other with a solution of chloromethyl methyl ether (10.6 mL, 0.14 mol) in THF (30 mL). With vigorous stirring, the two solutions were simultaneously added dropwise over 40 min. After stirring for 1 h, water was added, and the organic layer was separated and concentrated. The aqueous layer was extracted with CH_2Cl_2, and the extract was combined with the concentrated organic layer, washed with water, dried over Na_2SO_4, and evaporated. The residual colorless syrup slowly crystallized on standing. Yield: 23.4 g (0.092 mol, 92%).

5-Methoxymethoxybenzene-1,3-dicarboxylic acid monomethyl ester: The diester (33.1 g, 0.13 mol) was suspended in MeOH (650 mL), and aqueous NaOH (1 mol dm^{-3}, 120 mL, 0.12 mol) was added. The mixture was stirred at room temperature for 17 h. Water (100 mL) was added, and the mixture was concentrated to about 250 mL, upon which a white precipitate appeared. Extraction with EtOAc gave the unchanged diester. A solution of $KHSO_4$ (20.4 g, 0.15 mol) in water (100 mL) was slowly added to the aqueous layer. A colorless oil separated out, which gradually turned into a white solid. The solid was collected by filtration and washed with water. This crude material contains about 5% of the diacid, from which the desired monoacid was separated by Soxhlet extraction with CH_2Cl_2. Yield: 20.5 g (0.085 mol, 66%).

1: A solution of monoacid (6.88 g, 28.6 mmol) and Et_3N (4.39 mL, 31.5 mmol) in dry CH_2Cl_2 (50 mL) was cooled to 0°C. Isopropyl chloroformate (3.68 mL, 31.5 mmol) was added dropwise. After stirring for 2 h at 0°C, the reaction mixture was washed with iced water, ice-cooled dilute aqueous $KHSO_4$, and ice-cooled dilute aqueous $NaHCO_3$, dried, and evaporated. Evacuation of the obtained oil at 1 torr caused crystallization. This active ester was dissolved in THF (50 mL), cooled to 0°C, then an ice-cooled solution of $NaBH_4$ (3.25 g, 85.8 mmol) in water (15 mL) was added dropwise over 15 min, and the mixture was stirred for 15 min. After the usual workup, a colorless oil was obtained which slowly crystallized on standing overnight. Yield: 5.49 g (24.3 mmol, 85%). Caution: neat isopropyl chloroformate must be kept below 5°C during handling; warming to room temperature sometimes caused violent decomposition when a pipette or a syringe needle was dipped into it.

2: Methanesulfonyl bromide (2.28 mL, 28.5 mmol) was added dropwise to a solution of **1** (4.30 g, 19.0 mmol) and diisopropylethylamine (4.96 mL, 28.5 mmol) in CH_2Cl_2 (25 mL) at 0°C under N_2. The mixture was stirred for 22 h with gradual warming to room temperature. The resulting yellow solution was washed twice with water, dried, and evaporated. The resulting oil was purified by column chromatography (SiO_2, hexane/EtOAc = 7:3 *v*/*v*) to give a colorless oil, which slowly crystallized on standing. Yield: 4.76 g (67%).

3: A mixture of **2** (5.55 g, 19.2 mmol), 3,5-dihydroxybenzyl alcohol (1.28 g, 9.14 mmol), K_2CO_3 (5.31 g, 38.4 mmol), and [18]crown-6 (502 mg, 1.90 mmol) in acetone (60 mL) was heated to 80°C under argon for 3 h. After the usual workup, the product was purified by silica-gel column chromatography (hexane/EtOAc = 1:1 *v*/*v*). Repeated trituration in 2-propanol/hexane gave a white amorphous solid. Yield: 3.80 g (6.83 mmol, 75%).

4: A mixture of **3** (2.30 g, 4.13 mmol), sulfuric acid (12 mol dm^{-3} in water, 5 mL), MeOH (5 mL), and THF (10 mL) was stirred for 22 h at room temperature. After the usual workup, a colorless oil was obtained, which became a white amorphous solid on repeated trituration in $CHCl_3$/hexane. Yield: 2.01 g (4.27 mmol, 103%).

3,5-Bis(4-pentenyloxy)benzyl alcohol: A mixture of 5-bromo-1-pentene (3.28 g, 22 mmol), 3,5-dihydroxybenzyl alcohol (1.40 g, 10 mmol), K_2CO_3 (5.53 g, 40 mmol), KI (3.32 g, 20 mmol), and [18]crown-6 (0.53 g, 2 mmol) in acetone (10 mL) was heated at 90°C for 16 h. After the usual workup the product was purified by bulb-to-bulb distillation (1 torr, 220°C). Yield: 2.29 g (8.3 mmol, 83%).

3,5-Bis(4-pentenyloxy)benzyl bromide: Methanesulfonyl bromide (0.72 mL, 9.0 mmol) was added dropwise to a solution of the above alcohol (1.66 g, 6.0 mmol) and diisopropylethylamine (1.57 mL, 9.0 mmol) in CH_2Cl_2 (8 mL) at 0°C under N_2. The mixture was stirred for 9.5 h with gradual warming to room temperature. Tetraethylammonium bromide (0.63 g, 3.0 mmol) was added, and the mixture was stirred at room temperature for 6.5 h. The resulting yellow solution was washed twice with water, dried, evaporated, and purified by silica-gel column chromatography (hexane/EtOAc = 10:0–7:3 (*v*/*v*) followed by bulb-to-bulb distillation (1 torr, 260°C). Yield: 1.33 g (3.9 mmol, 65%).

5: A solution of pyrrole (670 mg, 10 mmol), 4′-methoxybiphenyl-4-carboxaldehyde (425 mg, 2.0 mmol), and 2,6-difluorobenzaldehyde (1.28 g, 9.0 mmol) in $CHCl_3$ (1 L) was bubbled with N_2 for 30 min, and $BF_3{\cdot}OEt_2$ (0.44 mL, 3.5 mmol) was added. The mixture was heated to 90°C for 6 h, then cooled to room temperature. 2,3-Dichloro-4,5-dicyano-1,4-benzoquinone (1.32 g, 5.8 mmol) was added, and the mixture was stirred for 12 h with protection from light. Triethylamine (0.50 mL, 3.6 mmol) was added, and the solvent was removed by rotary evaporation. The residue was treated with column chromatography (SiO_2, CH_2Cl_2), and red-violet fractions containing porphyrins were collected and evaporated. This mixture of porphyrins was dried in a vacuum, dissolved in dry CH_2Cl_2 (20 mL), and cooled to −78°C under N_2. Boron tribromide (0.50 mL, 5.3 mmol) in dry CH_2Cl_2 (6 mL) was added dropwise. The mixture was stirred at −78°C for 1 h, then warmed to 0°C over 3 h. Water was added, and the products were extracted with CH_2Cl_2, washed with dilute $NaHCO_3$ and water, dried, and evaporated. Purification by column chromatography (SiO_2, CH_2Cl_2/MeOH = 100:0–95:5) gave the desired monosubstituted porphyrin. Yield: 0.275 g (0.34 mmol, 14% based on pyrrole).

3,5-Bis(5-methoxymethoxy-3-methoxycarbonylbenzyloxy)benzyl bromide: Methanesulfonyl bromide (0.120 mL, 1.5 mmol) was added dropwise to a solution of **3** (557 mg, 1.0 mmol) and diisopropylethylamine (0.262 mL, 1.5 mmol) in CH_2Cl_2 (5 mL) at 0°C under N_2. The mixture was stirred for 16 h with gradual warming to room temperature. The resulting yellow solution was washed twice with water, dried, evaporated, and purified by column chromatography (SiO_2, hexane/EtOAc = 70:30 *v*/*v*) to give a white solid. Yield: 489 mg (79%).

6: A mixture of 3,5-bis(5-methoxymethoxy-3-methoxycarbonylbenzyloxy)benzyl bromide (76 mg, 0.12 mmol), **5** (100 mg, 0.12 mmol), K_2CO_3 (41 mg, 0.29 mmol), and [18]crown-6 (0.169 g, 0.639 mmol) in acetone (20 mL) was heated to 80°C for 3 h. After the usual workup (extraction with $CHCl_3$ instead of EtOAc), the product was treated with H_2SO_4 (12 mol dm^{-3}, 2 mL), MeOH (2 mL), and THF (5 mL) for 24 h at room temperature. After the usual workup (including extraction with $CHCl_3$ and neutralization with dilute $NaHCO_3$), the desired compound was purified by preparative GPC (t = 55 min). Yield: 97 mg (77 μmol, 62%).

7: A mixture of 3,5-bis(4-pentenyloxy)benzyl bromide (1.52 g, 4.49 mmol), **4** (1.00 g, 2.14 mmol), K_2CO_3 (1.48 g, 10.7 mmol), and [18]crown-6 (0.169 g, 0.639 mmol) in acetone (20 mL) was heated to 80°C for 2 h. After the usual workup, the product was purified by column chromatography (SiO_2, hexane/EtOAc = 70:30–50:50 *v*/*v*). Yield: 1.82 g (1.86 mmol, 87%).

8: Methanesulfonyl bromide (96 μL, 1.2 mmol) was added dropwise to a solution of **7** (610 mg, 0.62 mmol) and diisopropylethylamine (210 μL, 1.2 mmol) in CH_2Cl_2 (3 mL) at 0°C under N_2. The mixture was stirred for 22 h with gradual warming to room temperature. The resulting solution was washed twice with water, dried, and evaporated. The resulting yellow oil was purified by column chromatography (SiO_2, hexane/EtOAc = 70:30 *v*/*v*). Yield: 520 mg (0.50 mmol, 80%).

9: A mixture of **8** (270 mg, 0.26 mmol), **4** (60 mg, 0.13 mmol), K_2CO_3 (72 mg, 0.52 mmol), KI (86 mg, 0.52 mmol), and [18]crown-6 (69 mg, 0.26 mmol) in acetone (4 mL) was heated to 80°C for 1 h. After the

usual workup, the product was purified by preparative GPC ($t=48$ min). Yield: 223 mg (0.094 mmol, 72%).

Synthesis of the Reference Porphyrin

Bn-ZnPn: A mixture of **5** (50 mg, 61 μmol), benzyl bromide (9.5 μL, 80 μmol), K_2CO_3 (17 mg, 120 μmol), and [18]crown-6 (11 mg, 40 μmol) in acetone (1 mL) was heated to 80°C for 2 h. After the usual workup (extraction with $CHCl_3$), the product was converted to the zinc complex ($Zn(OAc)_2$ (66 mg, 300 μmol) in CH_3OH (1 mL) and $CHCl_3$ (5 mL), 80°C, 2 h), purified by preparative GPC ($t=58$ min), precipitated from CH_2Cl_2/CH_3OH, and washed with CH_3OH. Yield: 50 mg (52 μmol, 85%).

Synthesis of Dendrimer–Porphyrin Linked Compounds

G1$(CO_2Me)_2$-ZnPn: A mixture of **8** (84 mg, 80 μmol), **5** (81 mg, 100 μmol), K_2CO_3 (22 mg, 160 μmol), KI (27 mg, 160 μmol), and [18]crown-6 (21 mg, 80 μmol) in acetone (2 mL) was heated to 80°C for 2 h. After the usual workup (extraction with $CHCl_3$), the product was purified by preparative GPC ($t=50$ min), converted to the zinc complex ($Zn(OAc)_2$ (110 mg, 0.5 mmol) in $CHCl_3$ (6 mL) and CH_3OH (1 mL), 80°C, 2 h), precipitated from CH_2Cl_2/CH_3OH, and washed with CH_3OH. Yield: 93 mg (50 μmol, 62%).

G2$(CO_2Me)_6$-ZnPn: A mixture of **8** (189 mg, 180 μmol), **6** (114 mg, 90 μmol), K_2CO_3 (25 mg, 180 μmol), KI (30 mg, 180 μmol), and [18]crown-6 (30 mg, 90 μmol) in acetone (2 mL) was heated to 80°C. After 3 h, 20 mg of **8** (19 μmol) was added, and heating was continued for 1 h. After the usual workup (extraction with $CHCl_3$), the product was purified by preparative GPC ($t=46$ min), converted to the zinc complex ($Zn(OAc)_2$ (132 mg, 600 μmol) in $CHCl_3$ (6 mL) and CH_3OH (1 mL), 80°C, 2 h), precipitated from CH_2Cl_2/CH_3OH, and washed with CH_3OH. Yield: 167 mg (51 μmol, 57%).

G3$(CO_2Me)_{14}$-ZnPn: Methanesulfonyl bromide (55 μL, 685 mmol) was added dropwise to a solution of **9** (328 mg, 137 μmol) and diisopropylethylamine (120 μL, 685 μmol) in CH_2Cl_2 (3.5 mL) at 0°C under N_2. The mixture was stirred for 19 h with gradual warming to room temperature. Tetraethylammonium bromide (100 mg, 500 μmol) was added, and the mixture was stirred for 4 h. The resulting solution was washed twice with water, dried, and evaporated. The resulting yellow oil was purified by column chromatography (SiO_2, hexane/EtOAc = 70:30 *v/v*), and the colorless oil obtained (**10**: 264 mg, 107 μmol, 78%) was used in the next step. A mixture of **10** (234 mg, 95 μmol), **6** (60 mg, 47 μmol), K_2CO_3 (25 mg, 180 μmol), KI (30 mg, 180 μmol), and [18]crown-6 (24 mg, 90 μmol) in acetone (1 mL) was heated to 80°C for 3 h. After the usual workup (extraction with $CHCl_3$), the product was purified by preparative GPC ($t=43$ min), converted to the zinc complex ($Zn(OAc)_2$ (66 mg, 300 μmol) in $CHCl_3$ (3 mL) and CH_3OH (0.5 mL), 80°C, 3 h), precipitated from CH_2Cl_2/CH_3OH, and washed with CH_3OH. Yield: 104 mg (17.5 μmol, 36%).

G1$(Fc)_2$-ZnPn: $LiAlH_4$ (7.6 mg, 200 μmol) was added to a solution of G1$(CO_2Me)_2$-ZnPn (55 mg, 30 μmol) in dry THF (3 mL) at 0°C under N_2, and the mixture was stirred at 0°C for 2 h. Iced water (2 mL) and a cold aqueous solution of citric acid (1%, 20 mL) were added in this order, and the mixture was quickly extracted with $CHCl_3$. The extract was washed with cold dilute $NaHCO_3$, dried over Na_2SO_4, and evaporated. The violet residue was dissolved in dry CH_2Cl_2 (2 mL), and ferrocene carboxylic acid (23 mg, 0.10 mmol), EDC·HCl (29 mg, 0.15 mmol), and DMAP (36 mg, 0.30 mmol) were added. The mixture was stirred at room temperature under N_2 in the dark for 3 days. Water (5 mL) was added, and the mixture was extracted with CH_2Cl_2. The extract was washed with water (3 times), 1% citric acid (twice), dilute $NaHCO_3$ (twice), and water again. The organic layer was dried over Na_2SO_4, evaporated, and the product was purified by preparative GPC ($t=49$ min), precipitated from CH_2Cl_2/CH_3OH, and washed with CH_3OH. Yield: 56 mg (25 μmol, 84%).

G2$(Fc)_6$-ZnPn: This compound was prepared by the same procedure as G1$(Fc)_2$-ZnPn, by use of G2$(CO_2Me)_6$-ZnPn (98 mg, 30 μmol), THF (2 mL), and $LiAlH_4$ (17 mg, 450 μmol), then ferrocene carboxylic acid (62 mg, 270 μmol), EDC·HCl (52 mg, 270 μmol), DMAP (65 mg, 540 μmol), and CH_2Cl_2 (2 mL). The product was purified by preparative GPC ($t=46$ min), precipitated from CH_2Cl_2/CH_3OH, and washed with CH_3OH. Yield: 113 mg (26 μmol, 87%).

G3$(Fc)_{14}$-ZnPn: This compound was prepared by the same procedure as G1$(Fc)_2$-ZnPn, by use of G3$(CO_2Me)_{14}$-ZnPn (92 mg, 15 μmol), THF (3 mL), and $LiAlH_4$ (24 mg, 630 μmol), then ferrocene carboxylic acid (96 mg, 420 μmol), EDC·HCl (81 mg, 420 μmol), DMAP (101 mg, 840 μmol), and CH_2Cl_2 (3 mL). The product was purified by preparative GPC ($t=45$ min), precipitated from CH_2Cl_2/CH_3OH, and washed with CH_3OH. Yield: 56 mg (6.5 μmol, 43%).

Electrochemical Methods

Electrochemical measurements were carried out with an ALS/CHI Model 660 voltammetric analyzer under the following conditions: 0.1 mmol dm^{-3} in CH_2Cl_2 containing Bu_4NClO_4 (0.1 mol dm^{-3}), platinum electrode (0.1 mm diameter), platinum-wire counterelectrode, Ag/$AgClO_4$/CH_3CN reference electrode. The reference electrode was calibrated with a cyclic voltammogram of a solution of [$Fe(C_5H_5)_2$] (1 mmol dm^{-3} in CH_2Cl_2 with Bu_4NClO_4 (0.1 mol dm^{-3})), and all potentials are reported with reference to [$Fe(C_5H_5)_2$]. The DPV parameters are as follows: pulse amplitude 50 mV, potential increment 4 mV, pulse width 5–200 ms, pulse period 200 ms.

Picosecond Time-Resolved Fluorescence Measurements

Picosecond time-resolved fluorescence measurements were carried out with a streak camera system (C4334 and C5094, Hamamatsu). A kHz Ti/sapphire regenerative amplifier (Spitfire, Spectra-Physics) seeded by a Ti/sapphire mode-locked oscillator laser (Spectra-Physics, Tsunami) was used as the light source, and the second harmonic of the amplified pulse (400 nm, 0.35–13 nJ) was used for excitation. The polarization of the excitation and detection light was set at the magic angle. The time resolution of the measurements was 140 ps (full width at half maximum) with a sweep range of 10 ns. The fluorescence was collected with back-scattering geometry with respect to the excitation beam. All measurements were performed at room temperature. The sample solution was placed in a sealed 1-mm thick quartz cell after bubbling with N_2. Toluene (Uvasol, Merck) was used as the solvent. The concentrations of the sample solutions were 1.0 mM (Bn-ZnPn), 0.18 mM (G1$(Fc)_2$-ZnPn), 0.13 mM (G2$(Fc)_6$-ZnPn), and 0.12 mM (G3$(Fc)_{14}$-ZnPn).

Computational Methods

The initial geometries of the organic molecules were obtained by building the molecular model with the Chem3D program package (CambridgeSoft). The structure and coordinate files of the appropriate format were generated by a homemade program suite named PSFLIB. The atom types and force-field parameters of the porphyrin were determined by a similar method as that described for Mn porphyrins.[25] The choice of parameters for ferrocenes caused some difficulty; several groups reported force-field parameters of metallocenes with a dummy atom at the center of the cyclopentadienyl ring.[26] Although this approach gives a good representation of the rotation of cyclopentadienyl rings, it requires modification of the program code and thus is not handy. As we are not particularly interested in the detailed dynamics of the ferrocenyl groups themselves, we took the simplest model, in which all the cyclopentadienyl carbon atoms were bound to the iron atom by single bonds. The equilibrium bond lengths were taken from the crystal structure of ferrocenecarboxylic acid.[27] All other parameters were taken from the parm99 force field distributed with AMBER 7.[28] The RESP (restrained electrostatic potential fit) atomic charges[29] were obtained by quantum mechanical calculations (HF/6–31G*) with GAMESS (US),[30] followed by treatment with the RESP module of AMBER.

The MD calculation was performed with the NAMD package.[31] A time-step of 2 fs was used. The temperature was maintained by rescaling the velocities every 500 steps. The RATTLE constraint[32] was applied to all hydrogen atoms. A 10-Å cutoff was applied to nonbonding interactions. Simulation with explicit solvents was performed under periodic boundary conditions with a constant volume, and the long-range electrostatic forces were evaluated by the particle-mesh Ewald method.[33] The parameters

for the $CHCl_3$ solvent box were taken from Cieplak et al.[34] For simulations in the electrolyte solutions, a box with dimensions $118.4 \times 118.4 \times 118.4$ Å^3 was populated with one unit of the target molecule at the center and 100 units of $Bu_4N^+ClO_4^-$ at random positions, and the box was filled with $CHCl_3$ by use of the above solvent box. This gave the same concentrations of the target material (10^{-3} mol dm^{-3}) and the electrolyte (0.1 mol dm^{-3}) as in the experiments. Visualization of the resulting structures and trajectories were performed with VMD.[35] Calculations were performed on a Silicon Graphics SGI2800 computer of the Research Center of Computational Science (Okazaki Research Facilities, NINS) and a local cluster of Apple PowerMac G5 machines.

Acknowledgements

We thank Prof. Takuji Ogawa (IMS) for valuable discussions, Prof. Yuko Okamoto (Nagoya Univ.) for guidance in MD simulations, Mr. Seiji Makita (IMS) for elemental analysis and MALDI-TOF measurements, Ms. Michiko Nakano (IMS) for valuable help in NMR spectroscopic measurements, the IMS for the use of their LA500 NMR instrument, and the Research Center for Computational Science of Okazaki Research Facilities (NINS) for the use of their SGI2800 computer. This work was supported by a Grant-in-aid for Scientific Research in Priority Areas, "Reaction Control of Dynamic Complexes" (No. 16033262) of the Ministry of Education, Culture, Sports, Science, and Technology (MEXT) (Japan), a Grant-in-aid for Exploratory Research (No. 15655053) from the Japan Society for the Promotion of Science (JSPS), and the Nanotechnology Support Project of MEXT (Japan).

[1] a) G. R. Newkome, E. He, C. N. Moorefield, *Chem. Rev.* **1999**, *99*, 1689–1746; b) C. M. Casado, I. Cuadrado, M. Morán, B. Alonso, B. García, B. González, J. Losada, *Coord. Chem. Rev.* **1999**, *185–186*, 53–80; c) V. Balzani, P. Ceroni, A. Juris, M. Venturi, S. Campagna, F. Puntoriero, S. Serroni, *Coord. Chem. Rev.* **2001**, *219–221*, 545–572; d) E. Peris, *Coord. Chem. Rev.* **2004**, *248*, 279–297.

[2] a) B. Alonso, I. Cuadrado, M. Moran, J. Losada, *J. Chem. Soc. Chem. Commun.* **1994**, 2575–2576; b) I. Cuadrado, M. Moran, C. M. Casado, B. Alonso, F. Lobete, B. Garcia, M. Ibisate, J. Losada, *Organometallics* **1996**, *15*, 5278–5280; c) C. Valerio, J.-L. Fillaut, J. Ruiz, J. Guittard, J.-C. Blais, D. Astruc, *J. Am. Chem. Soc.* **1997**, *119*, 2588–2589; d) K. Takada, D. J. Diaz, H. D. Abruna, I. Cuadrado, C. Casado, B. Alonso, M. Moran, J. Losada, *J. Am. Chem. Soc.* **1997**, *119*, 10763–10773.

[3] a) J. Ruiz, C. Pradet, F. Varret, D. Astruc, *Chem. Commun.* **2002**, 1108–1109; b) S. Nlate, J. Ruiz, V. Sartor, R. Navarro, J.-C. Blais, D. Astruc, *Chem. Eur. J.* **2000**, *6*, 2544–2553.

[4] a) J. R. Aranzaes, C. Belin, D. Astruc, *Angew. Chem.* **2006**, *118*, 138–142; *Angew. Chem. Int. Ed.* **2006**, *45*, 132–136; b) D. Astruc, M.-C. Daniel, J. Ruiz, *Chem. Commun.* **2004**, 2637–2649.

[5] H. C. Yoon, M.-Y. Hong, H.-S. Kim, *Anal. Chem.* **2000**, *72*, 4420–4427.

[6] a) C. S. Rajesh, G. J. Capitosti, S. J. Cramer, D. A. Modarelli, *J. Phys. Chem. B* **2001**, *105*, 10175–10188; b) G. J. Capistosti, C. D. Guerrero, D. E. Binkley, Jr., C. S. Rajesh, D. A. Modarelli, *J. Org. Chem.* **2003**, *68*, 247–261; c) C. Kim, H. Kim. K. Park, *J. Polym. Sci. A: Polym. Chem.* **2004**, *42*, 2155–2161.

[7] a) C.-O. Turrin, J. Chiffre, D. de Moutauzon, G. Balavoine, E. Manoury, A.-M. Caminade, J.-P. Majoral, *Organometallics* **2002**, *21*, 1891–1897; b) C.-O. Turrin, J. Chiffre, D. de Montauzon, J.-C. Daran, A.-M. Caminade, E. Manoury, G. Balavoine, H.-P. Majoral, *Macromolecules* **2000**, *33*, 7328–7336.

[8] C. A. Christensen, L. M. Goldenberg, M. R. Bryce, J. Becher, *Chem. Commun.* **1998**, 509–510.

[9] N. Leventis, J. Yang, E. F. Fabrizio, A.-M. M. Rawashdeh, W. S. Oh, C. Soritiou-Leventis, *J. Am. Chem. Soc.* **2004**, *126*, 4094–4095.

[10] a) F. Loiseau, S. Campagna, A. Hameurlaine, W. Dahaen, *J. Am. Chem. Soc.* **2005**, *127*, 11352–11363; b) N. D. MacClenaghan, R. Passalacqua, F. Loiseau, S. Campagna, B. Verheyde, A. Hameurlain, W. Dahaen, *J. Am. Chem. Soc.* **2003**, *125*, 5356–5365.

[11] T. D. Selby, S. C. Blackstock, *J. Am. Chem. Soc.* **1998**, *120*, 12155–12156.

[12] J. Leveque, C. Moucheron, A. Kirsch-De Mesmaeker, F. Loiseau, S. Serroni, F. Puntoriero, S. Campagna, H. Nierengarten, A. Van Dorsselaer, *Chem. Commun.* **2004**, 878–879.

[13] a) T. Imaoka, R. Tanaka, S. Arimoto, M. Sakai, M. Fujii, K. Yamamoto, *J. Am. Chem. Soc.* **2005**, *127*, 13896–13905; b) T. Imaoka, H. Horiguchi, K. Yamamoto, *J. Am. Chem. Soc.* **2003**, *125*, 340–341.

[14] W. R. Dichtel, S. Hecht, J. M. J. Frechet, *Org. Lett.* **2005**, *7*, 4451–4454.

[15] Y. Kikuzawa, T. Nagata, *Bull. Chem. Soc. Jpn.* **2004**, *77*, 993–1000.

[16] G. Sieber, *Justus Liebigs Ann. Chem.* **1960**, *631*, 180–184 [*Chem. Abstr.* **1961**, *55*, 7625].

[17] K. L. Wooley, C. H. Hawker, J. M. J. Frechet, *J. Chem. Soc. Perkin Trans. 1* **1991**, 1059–1076.

[18] a) D. C. Tully, A. R. Trimble, J. M. J. Frechet, *Proc. SPIE-Int. Soc. Opt. Eng.* **2000**, *3999*, 1202; b) A. Dahan, M. Portnoy, *Macromolecules* **2003**, *36*, 1034–1038; c) W.-D. Jang, T. Aida, *Macromolecules* **2004**, *37*, 7325–7330.

[19] a) K. Hirotsu, K. Takabayashi, T. Kaneko, JP Patent 2003012661, **2003** [*Chem. Abstr.* **2003**, *138*, 90641]; b) K.-I. Furuhata, M. J. Kawamoto, *J. Appl. Polym. Sci.* **1997**, *64*, 2031–2036.

[20] a) A. J. Bard, L. R. Faulkner, *Electrochemical Methods: Fundamentals and Applications*, John Wiley and Sons, New York, **2001**, p. 290; b) A. J. Bard, L. R. Faulkner, *Electrochemical Methods: Fundamentals and Applications*, John Wiley and Sons, New York, **2001**, p. 194.

[21] A. E. Kaifer in *Transition Metals in Supramolecular Chemistry*, *NATO ASI Series* (Eds.: L. Fabbrizzi, A. Poggi), Kluwer, Dordrecht, **1994**, p. 227.

[22] C. M. Cardona, A. E. Kaifer, *J. Am. Chem. Soc.* **1998**, *120*, 4023–4024.

[23] a) Y. Rio, G. Accorsi, N. Armaroli, D. Felder, E. Levillain, J.-F. Nierengarten, *Chem. Commun.* **2002**, 2830–2831; b) S. Heinen, W. Meyer, L. Walder, *J. Electroanal. Chem.* **2001**, *498*, 34–43; c) L. L. Miller, B. Zinger, J. S. Schlechte, *Chem. Mater.* **1999**, *11*, 2313–2315.

[24] J. C. Smith, C. B. Gorman, *Polym. Mater. Sci. Eng.* **1999**, *80*, 316–317.

[25] P. Arnaud, K. Zakrzewska, B. Meunier, *J. Comput. Chem.* **2003**, *24*, 797–805.

[26] a) T. N. Doman, C. R. Landis, B. Bosnich, *J. Am. Chem. Soc.* **1992**, *114*, 7264–7272; b) P. Jungwirth, D. Stussi, J. Weber, *Chem. Phys. Lett.* **1992**, *190*, 29–35.

[27] F. Cotton, A. H. Reid, Jr., *Acta Cryst. Sect. C* **1985**, *C41*, 686–688.

[28] D. A. Case, D. A. Pearlman, J. W. Caldwell, T. E. Cheatham III, J. Wang, W. S. Ross, C. L. Simmerling, T. A. Darden, K. M. Merz, R. V. Stanton, A. L. Cheng, J. J. Vincent, M. Crowley, V. Tsui, H. Gohlke, R. J. Radmer, Y. Duan, J. Pitera, I. Massova, G. L. Seibel, U. C. Singh, P. K. Weiner, P. A. Kollman, Amber 7, University of California, San Francisco, San Francisco (USA), **2002**.

[29] C. I. Bayly, P. Cieplak, W. D. Cornell, P. A. Kollman, *J. Phys. Chem.* **1993**, *97*, 10269–10280.

[30] M. W. Schmidt, K. K. Baldridge, J. A. Boatz, S. T. Elbert, M. S. Gordon, J. H. Jensen, S. Koseki, N. Matsunaga, K. A. Nguyen, S. J. Su, T. L. Windus, M. Dupuis, J. A. Montgomery, *J. Comput. Chem.* **1993**, *14*, 1347–1363.

[31] a) A. C. Phillips, R. Braun, W. Wang, J. Gumbart, E. Tajkhorshid, E. Villa, C. Chipot, R. D. Skeel, L. Kale, K. Schulten, *J. Comput. Chem.* **2005**, *26*, 1781–1802; b) K. Schulten, "NAMD: Scalable Molecular Dynamics", to be found under http://www.ks.uiuc.edu/Research/namd/, **2006**.

[32] H. C. Andersen, *J. Comput. Phys.* **1983**, *52*, 24–34.

[33] T. Darden, D. York, L. Pedersen, *J. Chem. Phys.* **1993**, *98*, 10089–10092.

[34] a) P. Cieplak, J. W. Caldwell, P. A. Kollman, *J. Comput. Chem.* **2001**, *22*, 1048–1057; b) R. Bryce, "Amber Parameter Database", to be found under http://pharmacy.man.ac.uk/amber/, **2006**.
[35] a) W. Humphrey, A. Dalke, K. Schulten, *J. Mol. Graphics*, **1996**, *14*, 33–38; b) W. Humphrey, A. Dalke, K. Schulten ,"VMD: Visual Molecular Dynamics", to be found under http://www.ks.uiuc.edu/Research/vmd/, **2006**.

Received: April 29, 2006

